Characterization and Application of Nanomaterials (2021) Volume 4 Issue 1
doi:10.24294/can.v4i1.1291

Original Research Article

Preparation and characterization of magnetic graphene oxide nanocomposite ($GO\text{-}Fe_3O_4$) for removal of strontium and cesium from aqueous solutions

Sule Aytas[1], Sabriye Yusan[1*], Senol Sert[1], Cem Gok[2]

[1] *Institute of Nuclear Sciences, Ege University, 35100 Bornova, Izmir, Turkey. E-mail: sabriye.doyurum@ege.edu.tr*

[2] *Faculty of Technology, Department of Metallurgical and Materials Engineering, Pamukkale University, 20160 Kinikli Denizli, Turkey*

ABSTRACT

Magnetic graphene oxide nanocomposites (M-GO) were successfully synthesized by partial reduction co-precipitation method and used for removal of Sr(II) and Cs(I) ions from aqueous solutions. The structures and properties of the M-GO was investigated by X-ray diffraction, Fourier transformed infrared spectroscopy, X-ray photoelectron spectroscopy, transmission electron microscopy, scanning electron microscopy, vibrating sample magnetometer (VSM) and N_2-BET measurements. It is found that M-GO has 2.103 mg/g and 142.070 mg/g adsorption capacities for Sr(II) and Cs(I) ions, respectively. The adsorption isotherm matches well with the Freundlich for Sr(II) and Dubinin–Radushkevich model for Cs(I) and kinetic analysis suggests that the adsorption process is pseudo-second-ordered.

Keywords: Graphene Oxide; Magnetite; Nanocomposite; Strontium; Cesium, Sorption

ARTICLE INFO

Received: 26 January 2021
Accepted: 12 March 2021
Available online: 18 March 2021

1. Introduction

Nuclear and Industrial Safety Agency (Japan) reported that the Fukushima Daiichi reactor meltdowns have thus far released 15,000 tera becquerels of radioactive cesium-137 into the environment[1]. Also, strontium was measured in plant samples in four others villages, with values ranging from 12 to 61 Bq/kg for Sr-89 and 1.8 to 5.9 Bq/kg for Sr-90[2]. This accident caused a great environmental disaster for living metabolisms and plants. Furthermore, diverse anthropogenic activities like nuclear research reactors, the production and use of radioisotopes and radiopharmaceuticals bring about the spread of radioactive wastes in the environment[3].

Some radionuclides as cesium and strontium are biologically toxic and of great importance due to their long-lasting nature and high solubility in aqueous systems[4]. For this reason, it is a significant subject to find out efficient, economic method that can be used in the removal and recovery of cesium and strontium from contaminated environments. Different types of physicochemical methods as ion exchange, chemical precipitation, membrane separation and adsorption, etc. are used for removal and recovery of radionuclides. Considering many parameters, one of these techniques comes to the forefront. Adsorption is widely-used technique that is fast and effective approach in eliminating pollutants from aqueous solutions[5].

The most critical point in the development of new adsorption methods is developed new adsorbent materials. Among the previously developed adsorbents, nanomaterial and especially nano-composites have been received great attention owing to high adsorption capacity, selectivity, high surface area, fast kinetic performances, and reusability for several cycles use[6,7]. Furthermore, nano-engineered magnetic adsorbents can be widely applied in contaminant removal due to the magnetism and high surface area. The magnetic particles can be quickly separated from the water after adsorption and this provides easily controlled process[8].

In recent years, graphene oxide nanomaterials, which has a large theoretical surface area and high sorption capacity for the metallic cations, has with wide range of surface oxygen-containing functional groups such as hydroxyl, epoxy, and carboxyl[9,10]. According to literature, graphene oxide has a notable affinity toward hard and semi-hard cations like uranium, thorium, lanthanides, and also strontium. These superior properties make graphene oxide proper for efficient adsorbent of cesium and strontium. Unfortunately, disadvantage of the graphene oxide is colloidal behavior of its dispersion, which makes separation of its reaction products with metallic cations quite unfairable[9]. Preparation of composite is one of the possible solutions to solve this problem. In this study, magnetic-nano composites were synthesized by using graphene and also magnetite, which is economic and readily available material; on the other side it is not selective. Integration of these two materials solved agglomeration problem and chemical instability in acidic media[11,12]. Preparation of nano-composite material with graphene and magnetite, not only brings about the chemical resistance, but also increase adsorption capacity. In recent years, combining of magnetite and graphene into nanocomposites has become an important subject of research due to their new and/or enhanced functionalities that cannot be obtained by either component alone. So, this topic holds a great promise for a wide variety of applications in removal of contaminants from wastewater, surface enhanced Raman scattering, biomedical fields, catalysis, etc.[13,14]

In despite of various studies, there is lack of efficient, low cost, secure, high capacity, modifiable, dopeable and reusable technique about cesium and strontium removal from aqueous solution. Based on that, magnetic-nano graphene composites were synthesized and characterized to investigate the removability of radiotoxic strontium and cesium ions from aqueous solutions. Adsorption performance of prepared composite by batch experiment was studied by physicochemical parameters. The adsorption isotherm parameters were estimated by linear regression analysis, thermodynamic and kinetic parameters have been also calculated to clarify the adsorption mechanism. The interaction mechanism of cesium and strontium on the magnetic nano-composites was discussed from the experimental results.

2. Experimental procedure

2.1. Reagents and materials

The graphene oxide powder was purchased from the Sigma Aldrich. The stock standard solutions of strontium and cesium were prepared by dissolving an appropriate amount of $Sr(NO_3)_2$ (Merck) and $CsNO_3$ (Merck) in distilled deionized water. Considering the radioactivity of the ^{90}Sr, non-radioactive ^{88}Sr was used. All reagents used were of analytical reagent grade.

2.2. Instrumental and analytical conditions

The strontium and cesium concentration measurements were done using a Perkin-Elmer Optima 2000 DV ICP–OES. The shaking was carried out in a thermostated electronic shaker bath (GFL-1083 model).

To analyze the characteristics of the M-GO, scanning electron microscope (SEM, COXEM EM-30), transmission electron microscopy (TEM, FEI 120kV CTEM), Fourier transform infrared spectroscopy (FTIR, PERKIN ELMER SPECTRUM TWO), X-ray diffraction (XRD, Thermo Scientific ARL K-Alpha), X-ray photoelectron spectroscopy (XPS, Thermo Scientific Al K-Alpha), vibrating sample magnetometer (VSM, VSM550-100, Dexing Magnet Tech. Co) and N2-BET adsorption–desorption were

determined at 77 K using Micromeritics ASAP 2020.

2.3. Synthesis of M-GO

The M-GO nanocomposite was prepared by co-precipitation method, as reported in the literature[15]. 0.05 g graphene oxide powder was used during the synthesis of the nanocomposite.

2.4. Batch adsorption experiments

All sorption experiments were performed by the batch technique using 0.01 g of the sorbent suspended in 10 mL of strontium/cesium solution in a polyethylene (PE) flask at selected pH (2–9) and pH (2–12) for Sr(II) and Cs(I), respectively. The effects of sorption parameters such as contact time (15–300 min), Sr(II) concentration (10–50 mg/L), Cs(I) concentration (200–500 mg/L), adsorbent dosage (m/V) ratio (1–10) and temperature (25–45 °C) on the sorption of Sr(II)/Cs(I) were determined by changing a parameter and keeping others constant. The pH was adjusted by adding 0.1 mol/L HCl and NaOH to the solutions at the each experiment. After reaction, the solid and liquid was separated by the magnetic separation method. The concentrations of total Sr and Cs were determined by using ICP-OES. Each experiment was repeated three times and average values were used for calculation. The percentage sorption of metal ions from aqueous solution was computed as follows:

$$Adsorption\ (\%) = \frac{(C_i - C_e)}{C_i}\ x\ 100 \qquad (1)$$

where C_i and C_e are the initial and final metal ions concentration, respectively.

2.5 Kinetic studies

Kinetic studies were carried out in a thermostated shaker with polyethylene tubes at room temperature. In each run, 0.01 g of M-GO was added to 10 mL of Sr and Cs solution (50, 100, 150 mg/L and 200, 250, 300 mg/L), respectively and adjusted to the desired pH level. The contact time varied from 5 to 180 min. Samples were filtered from each tube at specified time intervals and analyzed for the remaining Sr/Cs ion concentrations by ICP-OES.

3. Results and discussion

3.1. Characterization

The micro-structure of the Fe_3O_4-GO(M-GO) was characterized by XRD (**Figure 1**). The peaks at 2θ values of 30.42°, 35.06°, 43.48°, 53.22°, 57.78° and 63.06° are the characteristic peaks of the Fe_3O_4 crystal with the cubic spinal structure for magnetic graphene nanocomposites matching well with those from the JCPDS card (19-0629) [16,17]. The small peak at 2θ = 26.5° corresponds to well-ordered graphene layers of GO skeleton and indicates that this way the formation of the magnetic composite as reported by other groups[18]. Generally we can conclude from the XRD pattern, the nanocomposite contains mostly Fe_3O_4 and it was synthesized with GO.

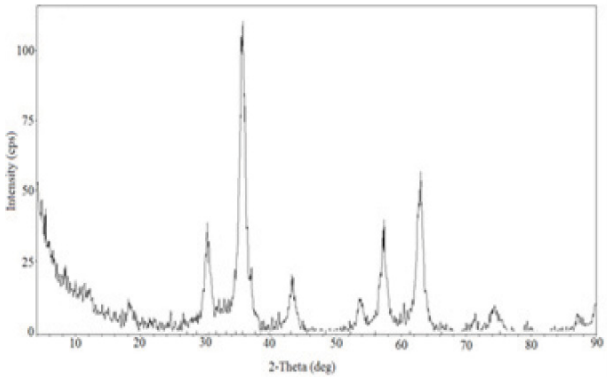

Figure 1. XRD pattern of M-GO.

SEM and TEM images of the obtained M-GO nanocomposite are showed in **Figure 2** and **Figure 3**. SEM images confirm the Fe_3O_4 nanoparticles are attached to the surface of the GO sheet in homogeneously. Nevertheless, TEM images of the M-GO shows that Fe_3O_4 nanoparticles are well decorated and clearly observed on the surface of graphene sheet.

XPS technique was used to verify the chemical state of M-GO and the results were shown in **Figure 4**. The wide scan XPS spectra of the M-GO shows the binding energy peaks about 285, 530 and 710 eV, which are attributed to C1s, O1s and Fe 2p, respectively[19,20]. In the figure spectrum, the peaks of Fe 2p 3/2 and Fe 2p 1/2 were located at about 711.12 and 724.79 eV, confirming that Fe_3O_4 was fairly synthesized on the GO.

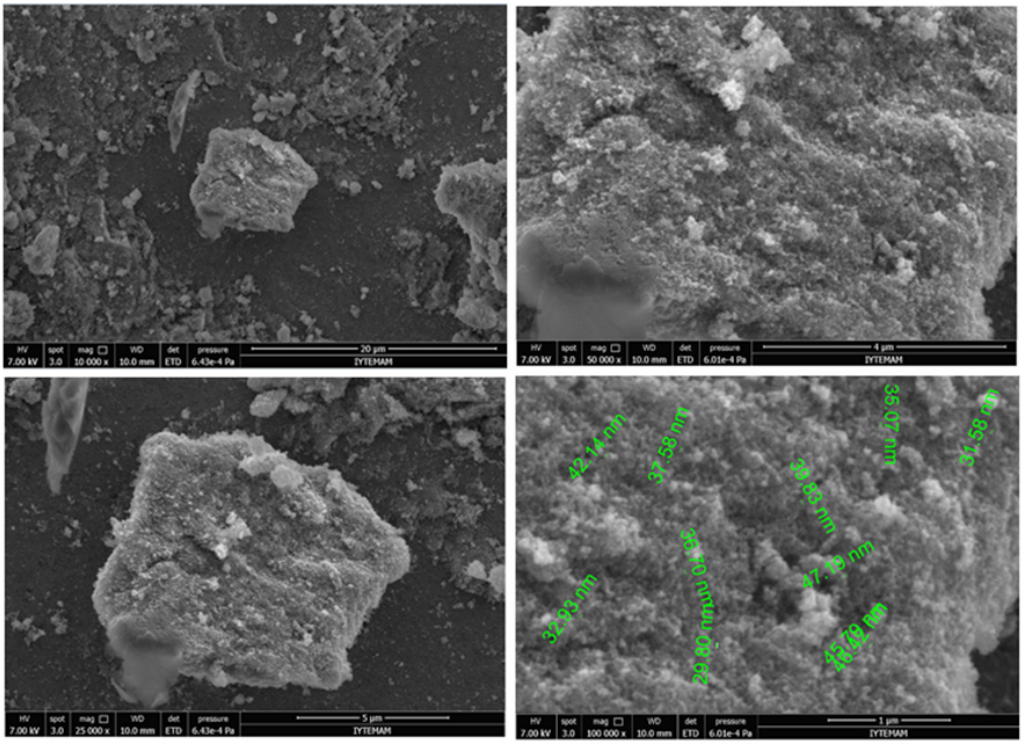

Figure 2. SEM image of M-GO.

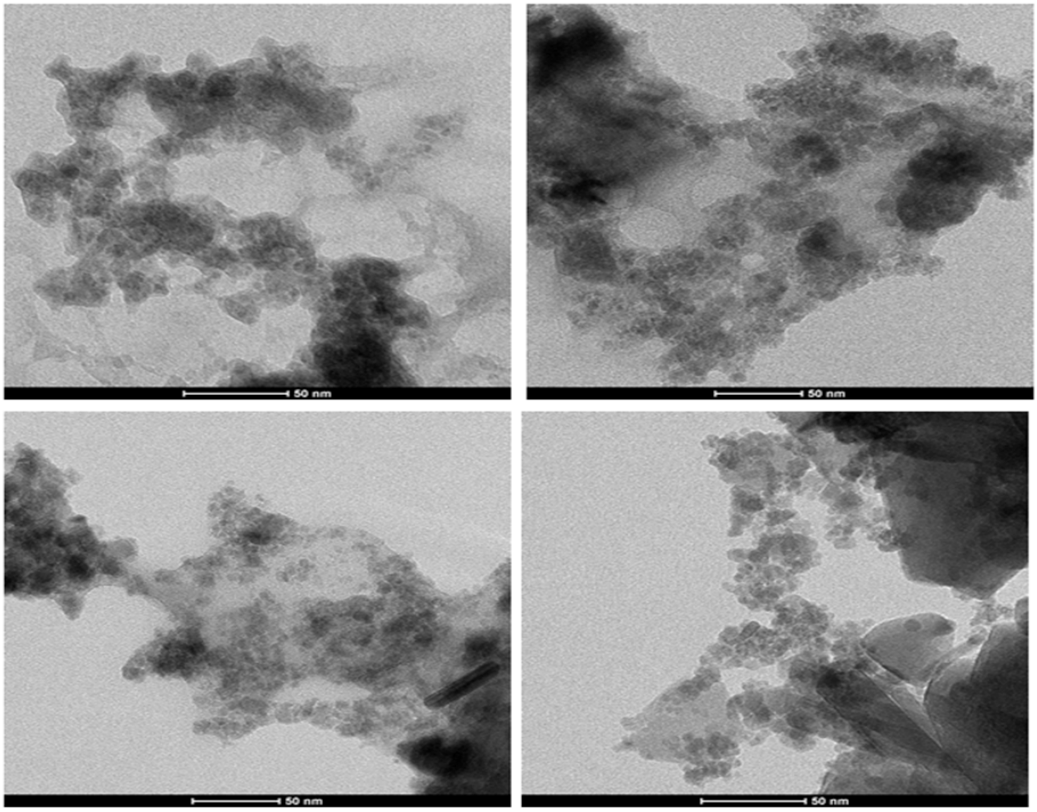

Figure 3. TEM image of M-GO.

The FT-IR spectrum of GO and M-GO is depicted in **Figure 5**. The GO sheet showed apparent adsorption bands for the carboxyl groups (stretching vibrations from C=O; 1,716 cm^{-1}), aromatic (C=C; 1,580 cm^{-1}), and alkoxy (stretching vibration from C–O (1,041 cm^{-1}). The intense peak at 1,415 cm^{-1} can

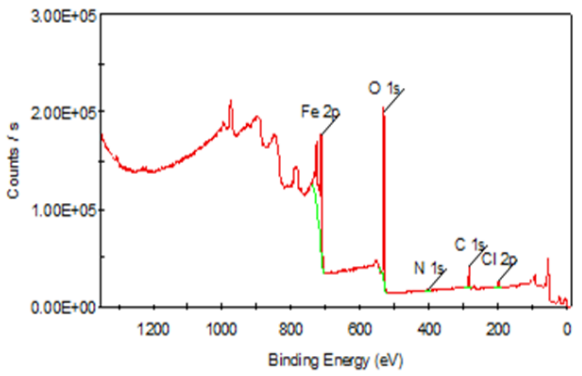

Figure 4. XPS survey scan spectrum of M-GO.

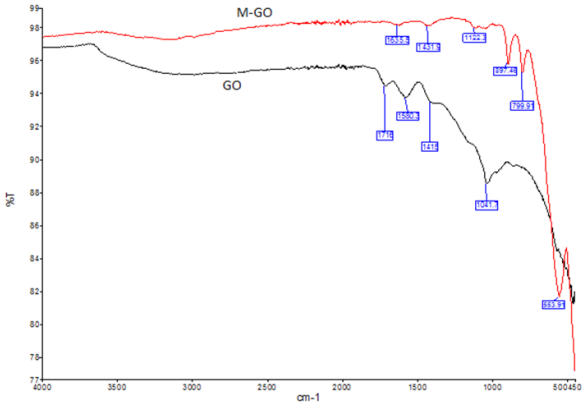

Figure 5. FT-IR spectra of M-GO.

be attributed to epoxy groups (C=C vibration) also showed at 1,122, 897 and 799 cm^{-1} in M-GO spectrum that related to symmetric stretching, asymmetric stretching, and deformation vibrations, respectively[18].

For M-GO, band at 1,635 cm^{-1} is assigned to H–O bending vibration. The peak at 553 cm^{-1} showed Fe–O bond from Fe_3O_4 The peak around 1,400 cm^{-1} can be explained by symmetric vibration of COO- groups which indicates the carboxylate groups of GO coordination with the iron cations[21].

The magnetic properties of the Fe_3O_4 nanoparticles, GO and the M-GO nanocomposite were determined at room temperature. The hysteresis loop of magnetite, GO and M-GO composite are shown in **Figure 6**, where the magnetization hysteresis loops appear S-like, and saturation magnetization is 16.16 and 10.74 emu/g for magnetite and M-GO, respectively. Nevertheless, as shown in the figure, GO sample has no magnetic property. The reduction in the saturation magnetization could be related to existence of GO and impurities on the surface of the magnetite nanoparticles[22]. However, M-GO still could be separated rapidly under the external magnet.

BET analysis was performed to investigate the specific surface area and pore size of the synthesized material. The BET surface area and pore size of M-GO was found as 124.37 m^2/g and 0.386 nm, respectively. In the literature, Cheng *et al.* and Hur *et al.* found the BET surface area for magnetic graphene oxide composites are 111. 8 m^2/g and 49.9 m^2/g, respectively[23,24]. The results obtained in this study are consistent with the literature.

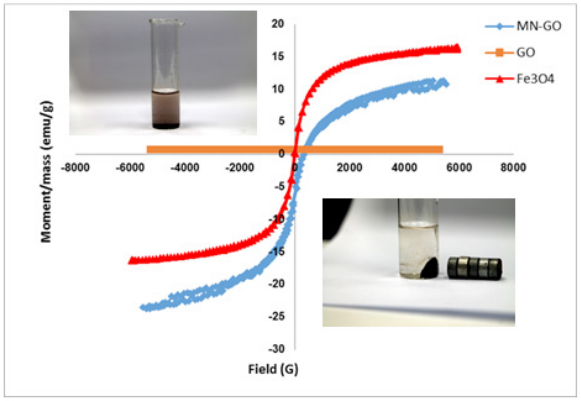

Figure 6. Magnetization versus magnetic field for magnetite, GO and M-GO.

3.2 Adsorption studies

3.2.1 pH effect

The pH value of solutions is a determining factor of the removal efficiency because it affects surface charge of the sorbent, and also the degree of ionization and speciation of the metal in solution. The effect of pH on Sr^{2+} and Cs^{+} adsorption is shown in **Figure 7 (a-b)**. As can be seen, the strontium and cesium removal on M-GO adsorbent are affected by the pH change of the solution. The maximum strontium and cesium uptake were found 40% at pH 4 and 17.92 mg Sr(II)/g and 59.5% at pH 10 and 148.77 mg Cs(I)/g as adsorbent, respectively. For this reason, pH 4 and pH 10 were used in subsequent experiments for Sr(II) and Cs(I), respectively. In addition, M-GO depicted higher adsorption capacity for Cs^{+} than for Sr^{2+} under the same experimental conditions. This can be attributed to the smaller hydrated ionic

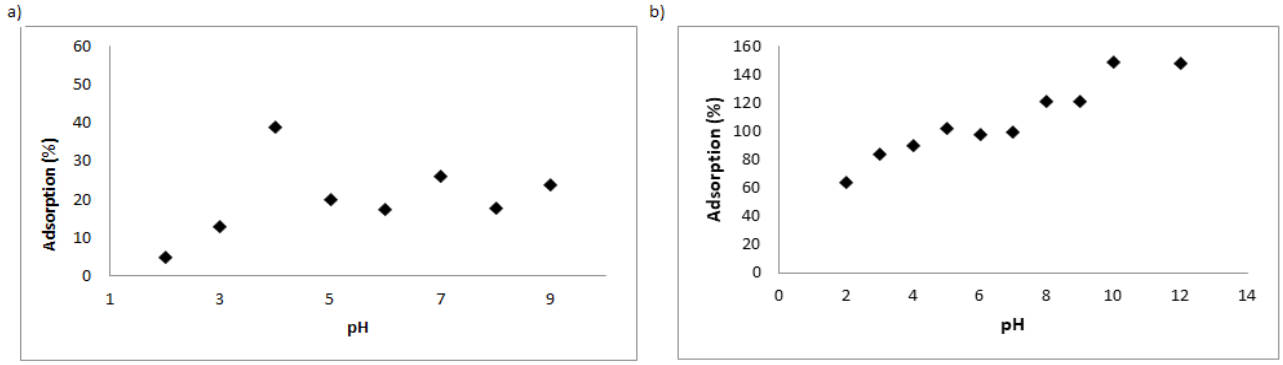

Figure 7. a) The effect of pH on the adsorption of Sr(II) ions with M-GO (c: 50 mg/L, m: 0.01 g, V: 10 mL, t: 120 min, T: 25 °C); **b)** The effect of pH on the adsorption of Cs(I) ions with M-GO (c: 250 mg/L, m: 0.01 g, V: 10 mL, t: 120 min, T: 25 °C).

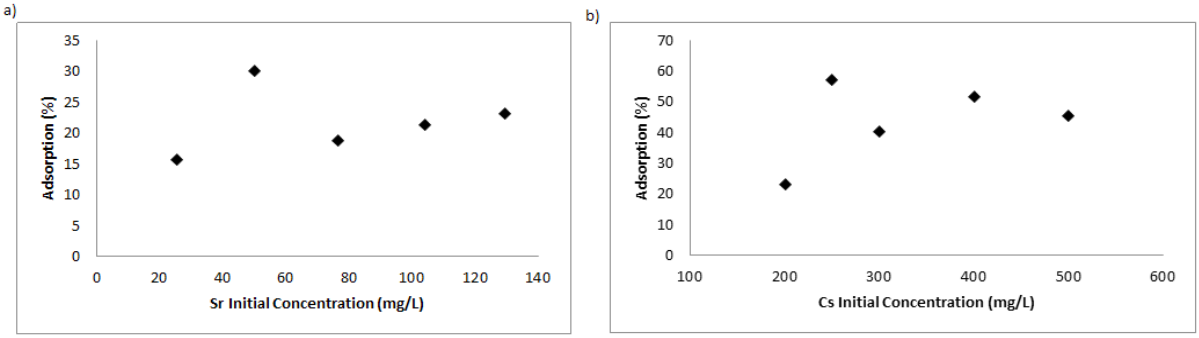

Figure 8. a) The effect of initial concentration on the adsorption of Sr(II) ions with M-GO (pH: 4, m: 0.01 g, V: 10 mL, t: 120 min, T: 25 °C); **b)** The effect of initial concentration on the adsorption of Cs(I) ions with M-GO (pH: 10, m: 0.01 g, V: 10 mL, t: 120 min, T: 25 °C).

radius of Cs^{+}[25].

3.2.2 Concentration effect

The Sr(II) and Cs(I) ions adsorption capacities of the M-GO were given as a function of the initial concentrations of metal ions in **Figure 8(a-b)**. The solution concentration of Sr(II) and Cs(I) was varied in the range 25–125 mg/L and 200–500 mg/L, respectively.

As shown in **Figure 8a**, when the strontium concentration increased, % adsorption value increased but the concentration value decreased from the 50 mg/L. The highest uptake for M-GO adsorbent was calculated as 29.98% at 50 mg/L strontium concentration. This concentration was used in subsequent parameter assays.

As shown in **Figure 8b**, when the cesium concentration increased, % adsorption value increased but the concentration decreased from 250 mg/L concentration to the equilibrium. The highest uptake for M-GO adsorbent was calculated as 57.2% at a cesium concentration of 250 mg/L. In subsequent parameter assays, this concentration has been studied at maximum adsorption.

3.2.3 Effect of dosage (m/V)

The adsorption of Sr(II) and Cs(I) ions decreases by increasing the ratio of the mass of the M-GO to volume of aqueous phase (m/V) (**Figure 9**). The highest values for the adsorption was obtained using 0.01 mL Sr/Cs solution and 0.01 g adsorbent (m/V) = 1 and it was taken as the optimum amount for other experiments for Sr and Cs adsorption. It can be concluded that low amount of nanocomposite can gives higher metals adsorption. Increasing the adsorbent dose above 1 g/L have a little or no change on Cs(I) removal while it can lead to significant removal for Sr(II).

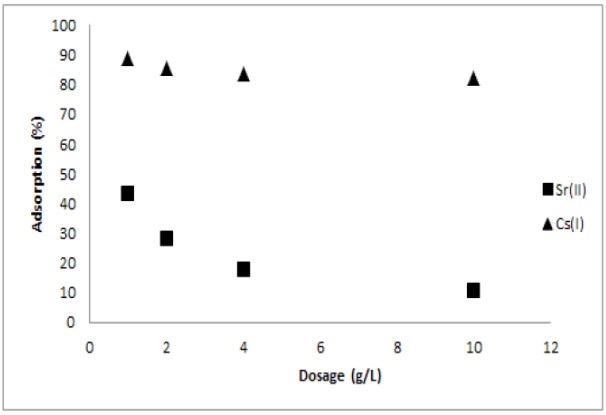

Figure 9. The effect of adsorbent dosage on the adsorption of Sr(II) and Cs(I) ions with M-GO (Sr; pH: 4, c: 50 mg/L, m: 0.01 g, V: 10 mL, t: 120 min, T: 25 °C: Cs; pH: 10, c: 250 mg/L, m: 0.01 g, V: 10 mL, t: 120 min, T: 25 °C).

3.3 Adsorption equilibrium and isotherm models

The adsorption process is a mass transfer operation that can be described mathematically by equilibrium and a rate process. The equilibrium is established between the concentration of the metal ions dissolved in aqueous phase and that bound to the adsorbent. The data obtained from experimental results is fundamental requirements for the design of adsorption systems. The data are used to develop equations and also to calculate isotherm parameters. By this way, the data, provide some insight into both the sorption mechanism and the surface properties and affinity of the sorbent can be used to compare different adsorbents under different operational conditions and to design and optimize an operating procedure[26–28]. In order to analyze the equilibrium data of the adsorption system, experimental data were fitted to Langmuir, Freundlich, Dubinin–Radushkevich, Temkin, Flory-Huggins and Brunauer, Emmer & Teller isotherms among the varied models. The constants of isotherm models along with correlation coefficients (R^2) have been calculated from the plots for adsorption of cesium and strontium on the composite material and the results are given in **Table 1**.

Adsorption equilibrium in the concentration range of 25–125 mg/L and 200–500 mg/L was studied with 10 mg of magnetic nanocomposite at 25 °C, 120 min contact time and pH 4 and 10.0 strontium and cesium, respectively.

The Langmuir isotherm, probably the most widely used model, assumes monolayer coverage of adsorbate over a homogeneous adsorbent surface[29]. The linear forms of the this model are expressed by the following equations:

$$\frac{C_e}{q_e} = \frac{1}{Q_0 b_L} + \frac{C_e}{Q_0} \quad (2)$$

where q_e is the amount of cesium and strontium ions adsorbed onto adsorbent; C_e is the equilibrium concentration of these metals in solution, and Q_0 and b_L are Langmuir constants related to adsorption capacity and adsorption energy, respectively. Q_0 and b_L were calculated from the slope and intercept of linear plots of C_e/q_e versus C_e.

The Freundlich model has been used to describe adsorption of strontium and cesium from solution onto composite material. This model is not restricted to the formation of the monolayer coverage. It is assumes an empirical expression encompassing the surface heterogeneity and the exponential distribution of the energy of active sites as well as multilayer adsorption. Linear form of Freundlich model can be represented as follows[30]:

$$\log q_e = \log K_F + \frac{1}{n_F} \log C_e \quad (3)$$

where K_F represents the adsorption capacity (mg/g), n_F is a constant related to adsorption intensity (dimensionless). The data obtained are well described by the Freundlich isotherm equation when plotted as $\log q_e$ versus $\log C_e$ (**Figure 10**).

Dubinin–Radushkevich is the other model that used extensively to determine the type of adsorption for the removal of strontium and cesium[31]. This model was used to calculate the apparent free energy of adsorption, proposed an equation to find out the adsorption mechanism on the basis of the potential theory assuming a porous structure of the sorbent and heterogeneous surface.

The linearized equation form of the D-R isotherm is given as:

$$\ln C_{ads} = \ln X_m - \beta\varepsilon^2 \quad (4)$$

where C_{ads} (mmol/g) is the amount of solute ad-

sorbed per unit weight of solid, X_m (mmol/g or mg/g) is the adsorption capacity, β (mol/K)^2 is a constant related to energy and ε is the Polanyi potential. Polanyi potential can be computed by the following equation:

$$\varepsilon = RT \ln\left(\frac{1}{1+C_e}\right) \quad (5)$$

where R is a gas constant in kJ/mol and T is the temperature in Kelvin. If $\ln C_{ads}$ is plotted against ε^2, β and X_m can be obtained from the slope and intercept, respectively (**Figure 11**). The adsorption mean energy (E), the free energy change when one mol of ion is transferred to the surface of the solid from infinity in the solution, is assumed by the following equation using the constant β:

$$E = \frac{1}{\sqrt{-2\beta}} \quad (6)$$

The Temkin isotherm model contains a factor that obviously assuming adsorbent–adsorbate interactions. This model takes into account that heat of adsorption of all molecules in the layer would decrease linearly rather than logarithmic with coverage by neglecting the extremely low and large value of concentrations[32]. The Temkin isotherm has generally been applied as follow:

$$q_e = \frac{RT}{b_{Te}} \ln a_{Te} + \frac{RT}{b_{Te}} \ln C_e \quad (7)$$

Where, b_{Te} is the constant of Temkin related to adsorption heat (J/mol); a_{Te} is the Temkin isotherm constant (L/mg); R is the gas constant and T is the absolute temperature (K). b_{Te} and a_{Te} constants were calculated from the intercept and slope of straight line of the plot of the q_e versus $\ln C_e$.

The Flory–Huggins isotherm model was examined to account for the degree of surface coverage characteristics of the sorbate on the sorbent[33,34]. The equation of the isotherm is as follows:

$$\frac{\Theta}{C_i} = K_{FH}(1-\Theta)^{n_{FH}} \quad (8)$$

Where, Θ is the degree of surface coverage, K_{FH} is the Flory–Huggins model equilibrium constant and n_{FH} is the Flory–Huggins model exponent. Θ is calculated using the following equation:

$$\Theta = 1 - \frac{C_e}{C_i} \quad (9)$$

The linearized equation of the model is given as:

$$\log\frac{\Theta}{C_i} = \log K_{FH} + n_{FH}\log(1-\Theta) \quad (10)$$

The constants of isotherm were extrapolated from plots of plot of $\log(\Theta/C_i)$ versus $\log(1-\Theta)$, and values of K_{FH} and n_{FH} calculated from the slope and intercept of the plot and are shown in **Table 1**. Equilibrium constant (K_{FH}) was used for the calculation of spontaneity of the Gibbs free energy (ΔG^0) on following equation:

$$\Delta G^0 = -RT \ln K_{FH} \quad (11)$$

The negative values of ΔG^0 confirmed the feasibility of the process and the spontaneous nature of adsorption ontoadsorbent.

Brunauer–Emmett–Teller (BET) isotherm model, related to the liquid–solid interface, is a theoretical equation, most widely applied in the gas–solid equilibrium systems[35]. This equation is presented as:

$$q_e = \frac{q_s C_{BET} C_e}{(C_s - C_e)\left[1 + (C_{BET} - 1)(C_e / C_s)\right]} \quad (12)$$

where C_{BET}, C_s, q_s and q_e are the BET adsorption isotherm constants relating to the energy of interaction with the surface (L/mg), adsorbate monolayer saturation concentration (mg/L), theoretical isotherm saturation capacity (mg/g) and equilibrium adsorption capacity (mg/g), respectively[36]. Linearized equation of the model is as follows:

$$\frac{C_e}{q_e(C_s - C_e)} = \frac{1}{q_s C_{BET}} + \frac{(C_{BET} - 1)}{q_s C_{BET}} \frac{C_e}{C_s} \quad (13)$$

The curve was plotted between $Ce/q_e(Cs–C_e)$ and C_e/C_s, and values of both constants q_s and C_{BET} were calculated from the intercept and slope. BET isotherm parameter for linear regression analyses and error functions are given in **Table 1**.

The high determination coefficients for linear

Table 1. Isotherm constants of models for strontium and cesium adsorption onto M-GO

Isotherm models	Parameters	Strontium	Cesium
Langmuir	Q_o (mg/g)	256.410	434.78
	b_L (L/mg)	0.004	0.035
	R^2	0.9249	0.2483
Freundlich	K_F (mg/g)	2.103	29.058
	n_F	0.772	1.973
	R^2	0.9987	0.4260
Dubinin–Radushkevich	X_m (mmol/g)	0.638	1.069
	β (mol/kJ)^2	2.10^{-4}	3.10^{-5}
	E (kJ/mol)	0.016	0.129
	R^2	0.8843	0.9611
Temkin	a_{TE} (L/g)	5.820	6.991
	b_{TE} (kJ/mol)	0.245	0.025
	R^2	0,9235	0.4867
Flory-Huggins	K_{FH}	$2.38.10^{-3}$	$3.93.10^{-5}$
	n_{FH}	1.190	1.860
	ΔG^0 (kj/mol)	14.972	25.142
	R^2	0.1920	0.5004
Brunauer, Emmer & Teller	q_s (mg/g)	3.753	39.745
	C_{BET} (L/mg)	0.421	2.020
	R^2	0.3481	0.5785

models show applicability of the model for metals adsorption using the present adsorbent. According to the correlation coefficients, the adsorption of strontium could be well described by Freundlich equation. Freundlich's model theory is regarded as the heterogeneous adsorption and the exponential distribution of the energy of active sites as well as multilayer adsorption. Dubinin and Radushkevich isotherm provide a particularly good model for the adsorption of cesium. This model has reported that the characteristics of sorption curve is related to the porous structure of the sorbent.

According to the results, the maximum adsorption capacities of strontium and cesium were calculated as 2.103 mg/g from Freundlich model and 142.07 mg/g from Dubinin–Radushkevich model, respectively (**Table 1**). The $1/n_F$ value between 0 and 1 indicates that the adsorption is favorable under the experimental conditions. As seen in **Table 1**, cesium adsorption on magnetic graphene composite was found high enough for separation. Moreover, the value of $1/n_F$ is known as heterogeneity factor and ranges between 0 and 1; the more heterogeneous the surface, the closer $1/n_F$ value is to 0. The numerical value of $1/n_F$ (< 1) indicates that adsorption capacity is only slightly suppressed at lower equilibrium concentration and the isotherm does not present any saturation of the solid surface of the sorbent by the sorbate[36].

One of the unique features of the Dubinin–Radushkevich isotherm model lies on the fact that it is temperature-dependent, which when adsorption data at different temperatures are plotted as a function of logarithm of amount adsorbed vs the square of potential energy, all suitable data will lie on the same curve, named as the characteristic curve[36]. The calculated E value is used to estimate the reaction mechanism of adsorption process. If value of E is smaller than 8 kJ/mol, it indicates a physical adsorption. If value of E is higher than 8 kJ/mol, the adsorption process is of a chemical nature. The E values obtained were 0.016 kJ/mol and 0.129 kJ/mol for strontium and cesium, respectively. Therefore, the magnitudes of E values are in the energy range of physical adsorption for strontium and cesium[7,8].

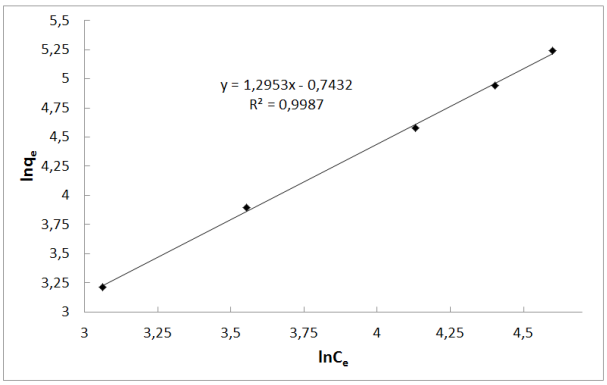

Figure 10. Linear isotherm models of Freundlich for strontium adsorption on magnetic graphene oxide composite.

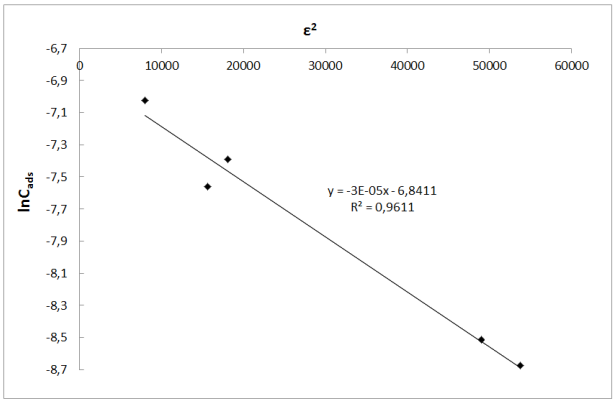

Figure 11. Linear isotherm models of Dubinin and Radushkevich for cesium adsorption on magnetic graphene oxide composite.

3.4 Kinetic parameters of adsorption

A study on the kinetics of adsorption is carrying out to obtain information about the adsorption mechanism, which is important for the efficiency of the process[37]. Therefore, two well-known kinetic equations were adopted to model the experimental data and identify the adsorption mechanism.

In order to analyze the sorption of Sr(II)/Cs(I) onto M-GO, the pseudo first equation and pseudo second order equation was employed[38–40]:

$$\log(q_e - q_t) = \log q_e - \frac{k_1 t}{2.303} \quad (14)$$

$$\frac{t}{q_t} = \frac{1}{k_2 q_e^2} + \frac{t}{q_e} \quad (15)$$

Where, q_e is the amount of metal ion adsorbed onto adsorbent at equilibrium (mg/g); q_t is the amount of metal ion adsorbed at various times; t (min) is the time of adsorption duration and k_1 is the first order rate constant (min^{-1}); k_2 (g/mol·min) is the second-order rate constant.

The experiments were conducted at different concentrations 50, 100, 150 ppm for Sr(II) and 200, 250, 300 ppm for Cs(I). From the slope ofeach linear trace, the rate constants were calculated and the results are presented in the **Table 2** and **Table 3** (pseudo-first-order model was not shown as figure because the R^2 values of the adsorption of Sr(II) and Cs(I) are low at the studied concentrations). The data obtained separately for each of the kinetic models from the slopes of plots show a good compliance with the pseudo second order equation. High R^2 values for the linear plots showed that kinetic data fitted the pseudo second order adsorption kinetic equation for Sr(II) and Cs(I) removal (**Figuer 12** and **Figure 13**).

The theoretical values of q_e for Sr(II) and Cs(I) removal also agree very well with the experimental ones. Both facts suggest that the adsorption of Sr(II) and Cs(I) onto M-GO follows the pseudo-second-order kinetic model. Therefore, the rate-limiting step may be chemical sorption or chemisorption through sharing or exchange of electrons between sorbent and adsorbate[5].

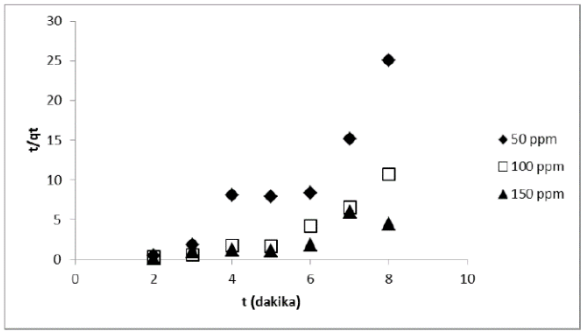

Figure 12. Pseudo-second-order plot for the adsorption of Sr(II) by M-GO.

Table 2. Rate parameters for the adsorption of Sr(II) onto M-GO at various initial concentrations

Concentration	50 ppm	100 ppm	150 ppm
Pseudo-first-order model			
q_e (mg/g)	1.8539	1.2600	4.5790
k_1 (1/min)	0.0999	0.0096	0.0145
R^2	0.0913	0.3406	0.0321
Pseudo-second-order model			
q^e (mg/g)	7.4404	16.7504	33.55
k_2 (g/mol·min)	1.1579	0.0627	1.1100
R^2	0.9646	0.9823	0.7632
Experimental q_e (mg/g)	7.89	18.22	32.30

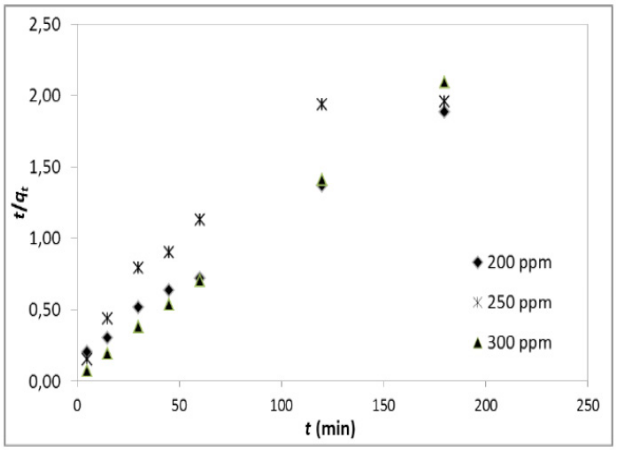

Figure 13. Pseudo-second-order plot for the adsorption of Cs(I) by M-GO.

Table 3. Rate parameters for the adsorption of Cs(I) onto M-GO at various initial concentrations

Concentration	200 ppm	250 ppm	300 ppm
Pseudo-first-order model			
q_e (mg/g)	69.47	100.74	120.46
k_1 (1/min)	0.0203	0.0205	0.0257
R^2	0.9586	0.7875	0.7567
Pseudo-second-order model			
q_e (mg/g)	104.17	96.15	86.96
k_2 (g /mol min)	0.0051	0.0003	0.0059
R^2	0.9965	0.8965	0.999
Experimental q_e (mg/g)	102.8	95.0	85.5

3.5 Thermodynamic studies

In this study, the adsorption of Sr(II) and Cs(I) onto M-GO was examined in the temperature range of 25–40 °C under optimized conditions (Sr: pH = 4, C: 50 mg/L, m/V: 1, t: 120 min; Cs: pH = 10, C: 250 mg/L, m/V: 1, t: 120 min and adsorbent amount of 0.01 g). **Figure 14 (a-b)** show the effect of temperature on the adsorption of Sr(II) and Cs(I) on the nanocomposite, respectively. Thermodynamic parameters like enthalpy change (ΔH^0), entropy change (ΔS^0) and free energy change (ΔG^0) were estimated using the following equations.

$$\ln K_d = \frac{\Delta S^0}{R} - \frac{\Delta H^0}{RT} \quad (16)$$

$$\Delta G^0 = \Delta H^0 - T\Delta S^0 \quad (17)$$

The enthalpy ΔH^0 (kJ/mol) and the entropy ΔS^0 (J/molK) of adsorption can be determined from the slope and the intercept of the linear fits which are gained by drawing $\ln K_d$ against $1/T$ respectively. The negative amounts ΔG^0 show that the adsorption process is spontaneous for both of the ions. The values are well under those related to chemical bond constitution, showing the physical property of the adsorption process[41]. Besides, the enthalpy variation ΔH^0 following adsorption is negative in all cases representing the exothermic nature of the adsorption. The results indicated that the reaction efficiency decreased as the temperature increased for Sr(II) removal but the reaction efficiency increased as the temperature increased for Cs(I) removal.

The negative value of ΔS^0 for Sr(II) shows the change in the randomness at the M-GO-solution interface during the adsorption. The entropy variations ΔS^0 of the system along with the adsorption of Cs(I) ions on the M-GO is positive in all cases, showing that more discover is generated following adsorption. The results were calculated in **Table 4**.

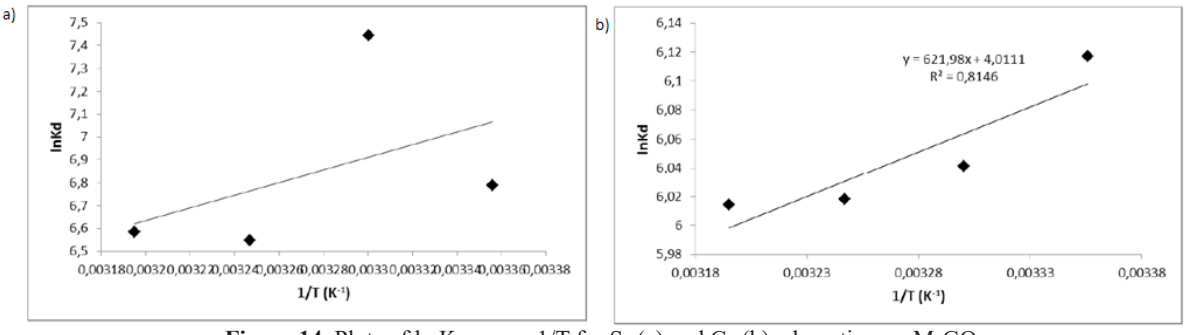

Figure 14. Plots of ln K_d versus 1/T for Sr (a) and Cs (b) adsorption on M-GO.

Table 4. Thermodynamic parameters for Sr(II) and Cs(I) sorption on M-GO as a function of temperature

M-GO	ΔH^o (kJ/mol)	ΔS^o (J/molK)	ΔG^o (kJ/mol)			
			298 K	303 K	308 K	318 K
Sr(II)	–22.97	–18.37	–17.49	–17.42	–17.33	–17.24
Cs(I)	–5.17	33.35	–15.11	–15.28	–15.44	–15.61

4. Conclusion

M-GO nanocomposite was synthesized using partial reduction co-precipitation method, which is simple, effective, economical and environmentally friendly technique for the removal of Sr(II) and Cs(I) from aqueous solutions. Prepared nanocomposite was characterized by SEM, TEM, XRD, FTIR, XPS and VSM. According to all characterization methods and literature data, we can conclude that M-GO was successfully prepared and possessed with the desired properties. The adsorption capacity of M-GO for Sr(II) and Cs(I) were found as 2.103 mg/g and 142.070 mg/g, respectively. Kinetic results indicated that the adsorption process could be defined by the pseudo-second-order kinetic model under the selected strontium and cesium concentration range which provides the best correlation of the data in all cases and the experimental q_e values agree with the calculated ones and the adsorption isotherm was fitted well to Freundlich model and D-R model for Sr(II) and Cs(I), respectively. The thermodynamic analysis of the sorption process for both of the radionuclides indicates that the system is spontaneous and exothermic. The values of ΔG^0 for Sr(II) and Cs(I) are well under those related to chemical bond constitution, showing the physical property of the adsorption process. It could be therefore concluded that the sorption mechanism was dominated by physisorption, but the overall observations suggest that the sorption process was administrated by combination of several mechanisms, such as physical sorption, ion exchange and complexation. Based on the results, M-GO can effectively remove the strontium and cesium ions from aqueous solutions.

Author contributions

Sule Aytas, Sabriye Yusan and Senol Sert performed the experiments and analyzed the data. Sule Aytas supervised and designed data. Sabriye Yusan and Cem Gok designed and analyzed data, and prepared the manuscript. Senol Sert realized ICP-OES measurements and also designed the manuscript.

Conflict of interest

The authors declare that they have no conflict of interest.

Acknowledgements

This research project was supported by Ege University Scientific Research Project Unit Project No. 2014 NBE 005.

References

1. Japan's Challenges Towards Recovery. Ministry of Economy, Trade and Industry [Internet]. [cited March 2012]. Available from: http://www.meti.go.jp/english/earthquake/nuclear/japan-challenges/pdf/japan-challenges_full.pdf.
2. IAEA Briefing on Fukushima Nuclear Accident [cited 13 April 2011]. Available from: https://www.iaea.org/newscenter/news/fukushima-nuclear-accident-update-log-17.
3. Tangestani F, Mallah MH, Rashidi A, Habibzadeh R. Adsorption of Cesium, Strontium, and Rubidium radionuclides in the Magmolecular process: The influence of important factors. Advances in Environmental Technology 2017; 3: 139–49.
4. Anzai, K, Ban N, Ozawa T, *et al.* Fukushima Daiichi Nuclear Power Plant accident: Facts, environmental contamination, possible biological effects, and countermeasures. Journal of Clinical Biochemistry & Nutrition 2012; 50(1): 2–8.
5. Yusan S, Gok C, Erenturk S, *et al.* Adsorptive removal of thorium (IV) using calcined and flux calcined diatomite from Turkey: Evaluation of equilibrium, kinetic and thermodynamic data. Applied Clay Science 2012; 67: 106–116.
6. Yusan SD, Akyil S. Sorption of uranium (VI) from aqueous solutions by akaganeite. Journal of Hazardous Materials2008; 160(2-3): 388–395.
7. Yusan S, Bampaiti A, Erenturk S, *et al.* Sorption of Th (IV) onto ZnO nanoparticles and diatomite-supported ZnO nanocomposite: Kinetics, mechanism and activation parameters. Radiochimica Acta 2016; 104(9): 635–647.
8. Gok C. Neodymium and samarium recovery by magnetic nano-hydroxyapatite. Journal of Radioanalytical and Nuclear Chemistry 2014; 301(3) :641–651.

9. Tayyebi A, Outokesh M, Moradi S, *et al.* Synthesis and characterization of ultrasound assisted "graphene oxide–magnetite" hybrid, and investigation of its adsorption properties for Sr(II) and Co(II) ions. Applied Surface Science 2015; 353: 350–362.
10. Yang H, Li H, Zhai J, *et al.* Magnetic prussian blue/graphene oxide nanocomposites caged in calcium alginate microbeads for elimination of cesium ions from water and soil. Chemical Engineering Journal 2014; 246: 10–19.
11. Jolivet J-P, Chanéac C, Tronc E. Iron oxide chemistry. From molecular clusters to extended solid networks. Cheminform 2004; 35(18): 481–483.
12. Chen S, Brown L, Levendorf M, *et al.* Oxidation resistance of graphene-coated Cu and Cu/Ni alloy. ACS Nano 2011; 5(2): 1321–1327.
13. Zhang Y, Chen B, Zhang L, *et al.* Controlled assembly of Fe3O4 magnetic nanoparticles on graphene oxide. Nanoscale 2011; 3: 1446–1450.
14. Yao Y, Miao S, Liu S, *et al.* Synthesis, characterization, and adsorption properties of magnetic Fe_3O_4 @ graphene nanocomposite. Chemical Engineering Journal 2012; 184: 326–332.
15. Yusan S, Korzhynbayeva K, Aytas S, *et al.* Preparation and investigation of structural properties of magnetic diatomite nanocomposites formed with different iron content . Journal of Alloys & Compounds 2014; 608: 8–13.
16. El-din TAS, Elzatahry AA, Aldhayan DM, *et al.* Synthesis and characterization of magnetite zeolite nano composite. International Journal of Electrochemical Science 2011; 6: 6177–6183.
17. Chen L, Xu J, Hu J. Removal of U(VI) from aqueous solutions by using attapulgite/iron oxide magnetic nanocomposites. Journal of Radioanalytical & Nuclear Chemistry 2013; 297(1): 97–105.
18. Nodeh HR, Ibrahim WAW, Ali I, *et al.* Development of magnetic graphene oxide adsorbent for the removal and preconcentration of As(III) and As(V) species from environmental water samples. Environmental Science and Pollution Research 2016; 23: 9759–773.
19. Guo J, Wang R, Tjiu WW, *et al.* Synthesis of Fe nanoparticles @ graphene composites for environmental applications. Journal of Hazardous Materials 2012; 225-226: 63–73.
20. Qin Y, Long M, Tan B, *et al.* RhB adsorption performance of magnetic adsorbent Fe_3O_4/RGO composite and its regeneration through a Fenton-like reaction. Nano-Micro Letters 2014; 6(2): 125–135.
21. Lujaniene G, Semcuk S, Lecinskyte A, *et al.* Magnetic graphene oxide based nano-composites for removal of radionuclides and metals from contaminated solutions. Journal of Environmental Radioactivity 2017; 166(1): 166–174.
22. Dorniani D, Bin Hussein MZ, Kura AU, *et al.* Preparation of Fe_3O_4 magnetic nanoparticles coated with gallic acid for drug delivery. International Journal of Nanomedicine 2012; 7: 5745–5756.
23. Cheng, G, Yu, X, Zhou M, *et al.* Preparation of magnetic graphene composites with hierarchical structure for selective capture of phosphopeptides. Journal of Materials Chemistry B 2014; 2(29): 4711–4719.
24. Hur J. Shin J, Yoo J, Seo Y-S. Competitive adsorption of metals onto magnetic graphene oxide: Comparison with other carbonaceous adsorbents. The Scientific World Journal 2015: 836287.
25. Kakutani Y, Weerachawanasak P, Hirata Y, *et al.* Highly effective K-Merlinoite adsorbent for removal of Cs^+ and Sr^{2+} in aqueous solution. RSC Advances 2017; 7: 30919–30928.
26. Khambhaty Y, Mody K, Basha S, *et al.* Kinetics, equilibrium and thermodynamic studies on biosorption of hexavalent chromium by dead fungal biomass of marine Aspergillus niger. Chemical Engineering Journal 2009; 145: 489–495.
27. Khani MH. Statistical analysis and isotherm study of uranium biosorption by Padina sp. algae biomass. Environmental Science & Pollution Research 2011; 18: 790–799.
28. Gok C, Aytas S. Recovery of thorium by high-capacity biopolymeric sorbent. Separation Science and Technology 2013;48(14): 2115–2124.
29. Langmuir I. The adsorption of gases on plane surfaces of glass, mica and platinum. Journal of Chemical Physics 2015; 40(9): 1361–1403.
30. Freundlich H. Adsorption in solution. Journal of Physical Chemistry 1906; 57: 384–410.
31. Dubinin MM. The potential theory of adsorption of gases and vapors for adsorbents with energetically non-uniform surface. Chemical Reviews 1960; 60:

235–266.
32. Temkin MJ, Pyzhev V. Recent modifications to Langmuir isotherms. Acta Physiochim 1940; 12: 217–222.
33. Flory PJ. Thermodynamics of high polymer solutions. Journal of Chemical Physics 1942; 10: 51–62.
34. Huggins ML. Some properties of solutions of long-chain compounds. Journal of Chemical Physics 1942; 10: 151–158.
35. Bruanuer S, Emmett PH, Teller E. Adsorption of gases in multimolecular layers. Journal of the American Chemical Society 1938; 60: 309–316.
36. Foo KY, Hameed BH. Insights into the modeling of adsorption isotherm systems. Chemical Engineering Journal 2010; 156: 2–10.
37. Jain AK, Gupta VK, Bhatnagar A, *et al.* Utilization of industrial waste products as adsorbents for the removal of dyes. Journal of Hazardous Materials 2003; B101: 31–42.
38. Lagergren S. Zur theorie der sogenannten adsorption geloster stoffe. Kungliga Svenska Vetnskapsakademiens. Handlingar 1898; 24(4): 1–39.
39. Ho YS, Mckay G. The kinetics of sorption of basic dyes from aqueous solution by sphagnum moss peat. The Canadian Journal of Chemical Engneering 1998; 76: 822–827.
40. Liang S, Guo X, Feng N, *et al.* Isotherms, kinetics and thermodynamic studies of adsorption of Cu^{2+} from aqueous solutions by Mg^{2+}/K^{+} type orange peel adsorbents. Journal of Materials Chemistry 2010; 174: 756–762.
41. Almeida CAP, Debacher NA, Downs AJ, *et al.* Removal of methylene blue from colored effluents by adsorption on montmorillonite clay. Journal of Colloid and Interface Science 2009; 332(1): 46–53.